

# Recent Advances in n-Type Thermoelectric Nanocomposites

Junhui Tang, Yanling Chen, Samantha R. McCuskey, Lidong Chen,\* Guillermo C. Bazan,\* and Ziqi Liang\*

Organic/inorganic thermoelectric nanocomposites (TENCs) have seized great attention because they integrate the advantages of inorganic (i.e., high electrical conductivity) and organic (i.e., low thermal conductivity and mechanical flexibility) components. Major barriers that obstruct the development of this field are the lack of n-type TE materials and their relatively low performance, leaving the construction of TE devices difficult to realize. This review article is therefore focused on recent advances on n-type TENCs that primarily comprise carbon nanotube (CNT) and inorganic nanocrystal (NC)-based hybrids. CNT-based n-type TENCs are fabricated mainly by transforming the p-type CNT to n-type with organic dopants or by blending CNTs with n-type semiconducting polymers. NC-based n-type TENCs are typically obtained by blending semiconductor nanocrystals or metallic nanostructures with polymers. Additionally, the fabrication and thermoelectric performance of 2D layered superlattice structures are also reviewed. Finally, an outlook of n-type TENCs is given with a perspective for their possible future improvements.

heat; hence, it is essential to make use of this waste heat. Thermoelectric (TE) materials enable us to realize the direct transformation between heat and electricity based on the Seebeck effect and Peltier effect, respectively.<sup>[5]</sup> Thus, as a new type of energy conversion technology, TE conversion technology can recover energy from waste heat, thereby effectively improving the efficiency of energy utilization. To evaluate the performance of TE materials, a dimensionless figure of merit ( $zT$ ) is introduced, which is defined as Equation (1)<sup>[6,7]</sup>

$$zT = \frac{S^2 \sigma T}{\kappa} \quad (1)$$

In Equation (1),  $S$  represents the Seebeck coefficient ( $V K^{-1}$ ),  $\sigma$  is the electrical conductivity ( $S m^{-1}$ ),  $T$  is the absolute temperature (K), while  $\kappa$  refers to the thermal

conductivity ( $W m^{-1} K^{-1}$ ). Additionally,  $S^2 \sigma$  ( $W m^{-1} K^{-2}$ ) is generally denoted as the power factor (PF). It is worth noting that these parameters are intimately coupled to each other.<sup>[5,8]</sup> Therefore, a trade-off has to be made to obtain a high  $zT$  in TE materials.

Traditional inorganic TE materials, such as SiGe,<sup>[9]</sup> PbTe,<sup>[10]</sup> and Bi<sub>2</sub>Te<sub>3</sub>,<sup>[11]</sup> have made enormous advances during the past decades, presenting high  $zT$  values and showing great application potential. However, these materials have brittle, heavy, and toxic properties, which hinder their application in daily life. Besides, considering the relative scarcity of some of these elements in earth's crust, the cost of these inorganic bulk materials is so high that they may not be suitable for large-area manufacturing. Moreover, the fabrication methods include ball-milling and hot-pressing processes, which consume a large amount of energy and undermine the significance of utilizing waste heat. By contrast, organic thermoelectric (OTE) materials have recently received great attention because they display superiorities such as flexibility, low-cost, lightweight, low-temperature solution processing, and flexible molecular design for enhancing TE performance.<sup>[3,12]</sup> In spite of these advantages, the electrical conductivity of OTEs is significantly lower than that of their inorganic counterparts even after effective doping.<sup>[13]</sup> Therefore, the strategy of fabricating organic–inorganic thermoelectric nanocomposites (TENCs) by combining the intrinsic high electrical conductivity of inorganic components and the low thermal conductivity of organic components illuminates the great potential for developing high- $zT$  TE materials.<sup>[14]</sup> Moreover, the abundant interfaces created in TENCs can introduce phonon-boundary scattering and effectively reduce the lattice thermal conductivity.<sup>[15]</sup>

## 1. Introduction

The past decade has witnessed increasing energy shortage issues, necessitating the development of environmentally friendly clean energy and the improvement of existing energy efficiency.<sup>[1–4]</sup> Most of the energy is dissipated in the form of

J. Tang, Prof. Z. Liang  
 Department of Materials Science  
 Fudan University  
 Shanghai 200433, China  
 E-mail: zqliang@fudan.edu.cn

Y. Chen, Prof. L. Chen  
 State Key Laboratory of High Performance Ceramics  
 and Superfine Microstructure  
 Shanghai Institute of Ceramics  
 Chinese Academy of Sciences  
 Shanghai 200050, China  
 E-mail: cld@mail.sic.ac.cn

Y. Chen  
 Center of Materials Science and Optoelectronics Engineering  
 University of Chinese Academy of Sciences  
 Beijing 100049, China

S. R. McCuskey, Prof. G. C. Bazan  
 Department of Chemistry and Biochemistry & Department  
 of Materials Science  
 University of California at Santa Barbara  
 Santa Barbara, CA 93106-9510, USA  
 E-mail: bazan@chem.ucsb.edu

 The ORCID identification number(s) for the author(s) of this article can be found under <https://doi.org/10.1002/aelm.201800943>.

DOI: 10.1002/aelm.201800943

To fabricate a TE module, both p- and n-type TE materials are required yet most of the existing research focuses on p-type materials. Additionally, the TE performance of n-type TENCs lags far behind that of p-type counterparts.<sup>[16]</sup> More importantly, n-type TE materials are generally unstable in air due to their electron-rich characteristics. Thus, this review article aims to center on the n-type TENCs, comprising the blends of either carbon nanotubes (CNTs) or inorganic nanocrystals (NCs) with organic materials. Recent advances in n-type CNT- and NC-based TENCs are presented, and their TE performance parameters are summarized in **Tables 1** and **2**, respectively. In particular, the doping mechanisms of CNT-based n-type TENCs are elucidated. A variety of effective strategies for enhancing the TE performance in n-type TENCs are highlighted. Finally, a conclusion is drawn with regard to the difference between CNT- and NC-based n-type TENCs. Furthermore, an outlook of n-type TENCs improvement is given, including their ambient stability, the influence of organic/inorganic heterointerfaces on TE performance, the method of precisely controlling the film morphology, as well as notably reducing the content of inorganic components while maintaining high PFs.

## 2. Organic:Carbon Nanotube Blends

Carbon nanotubes are often used as fillers for thermoelectric nanocomposites due to their excellent electrical and mechanical properties.<sup>[17]</sup> Extensive studies have been performed on the TE performance of pure carbon nanotubes and their p-type nanocomposites.<sup>[18–20]</sup> This interest can be ascribed to the intrinsic p-type characteristics of pristine CNTs. Doping by oxygen in air during synthesis and storage, as well as the presence of hydroxyl and carboxyl functionalities on the surface of CNTs, are the main reasons for their p-type behavior.<sup>[21]</sup> Substantial efforts have also been dedicated to make n-type CNTs, including by reaction with alkali metals and by including nitrogen atoms through chemical vapor deposition (CVD) synthesis. To make n-type TENCs, CNTs are usually either reduced or blended with n-type organic semiconductors, including organic small molecules and polymers. Meanwhile, the air stability of these n-type TENCs has also been a research focus.<sup>[22,23]</sup>

### 2.1. Transformation of CNTs from p- to n-Type

One commonly used method to obtain n-type CNT-based TENCs is to treat pristine CNTs with reducing agents, such as hydrazine,<sup>[24,25]</sup> calcium hydride (CaH<sub>2</sub>),<sup>[26]</sup> or sodium borohydride (NaBH<sub>4</sub>),<sup>[27]</sup> as well as organic molecules containing amine groups, e.g., polyethylenimine (PEI)<sup>[22,28]</sup> and diethylenetriamine (DETA).<sup>[29]</sup> These reactions switch the major charge carrier type from holes to electrons.

In 2011, Blackburn and co-workers found that hydrazine was an effective n-type dopant for CNTs because hydrazine physisorbed on the surface would donate a large amount of electrons into metallic CNTs and their semiconducting analogs.<sup>[25]</sup> They also reported that hydrazine was a better dopant than other amine-containing molecules such as methylamine, ethylenediamine, and PEI, and would raise the Fermi level 0.7 eV



**Junhui Tang** graduated with a B.S. in Materials Chemistry from Fudan University in 2018. He is currently a graduate student in the group of Prof. Ziqi Liang at Fudan University. His research areas focus on organic and hybrid thermoelectrics.



**Yanling Chen** graduated with a B.S. in Materials Science and Engineering from Fuzhou University in 2014. She is currently a Ph.D. candidate at Shanghai Institute of Ceramics, Chinese Academy of Sciences under the supervision of Prof. Lidong Chen. Her research areas focus on organic thermoelectrics.



**Ziqi Liang** obtained his Ph.D. in Polymer Science in the Department of Materials Science and Engineering at Pennsylvania State University in March 2006. He then pursued postdoctoral work at the University of Cambridge from May 2006 to 2008. In June 2008, he joined the National Research Energy Laboratory as a postdoctoral researcher, later to become Scientist III. In September 2012, he joined the Department of Materials Science at Fudan University as a Professor. Currently, Prof. Liang's group conducts research on organic and perovskite solar cells, as well as organic and hybrid thermoelectrics.

higher than intrinsic CNTs. Moreover, the sheet resistance of hydrazine-treated CNT thin films could be tailored to match what was observed with the p-type counterparts. Interestingly, although the doping efficiency of PEI-doped CNTs was not as high as that of hydrazine-doped analogs, PEI could surpass the air stability of hydrazine-doped films. More importantly, given the issues of toxicity, storage difficulty, and air instability of hydrazine, PEI has been more extensively reported in the literature. For instance, the Yu group decorated single-walled carbon nanotubes (SWCNTs) with PEI, which was physically absorbed on the surface of CNTs via a thermally activated process.<sup>[28]</sup> After stirring with PEI solution at 50 °C for 3 days, the SWCNTs

**Table 1.** Summary of the TE performance of n-type carbon nanotube-based TENCs.

TENCs	Preparation method	$\sigma$ [S cm <sup>-1</sup> ]	$S$ [ $\mu$ V K <sup>-1</sup> ]	PF [ $\mu$ W m <sup>-1</sup> K <sup>-2</sup> ]	$\kappa$ [W m <sup>-1</sup> K <sup>-1</sup> ]	$zT$	Ref.
CNTs/PEI	Drop immersion	30	-57	9.7	N/A	N/A	[27]
CNTs/PEI-NaBH <sub>4</sub>	Drop immersion	60	-77	35.6	N/A	N/A	[27]
CNTs/PEI/DETA	Vacuum filtration	39	-63	15.5	N/A	N/A	[29]
CNTs/PEI/DETA-NaBH <sub>4</sub>	Vacuum filtration	52	-86	38	N/A	N/A	[29]
SWCNT/DETA-CaH <sub>2</sub>	Vacuum filtration	165	-41	27.7	N/A	N/A	[26]
DWCNT-PEI/graphene-PVP	LbL assembly	300	-80	190	N/A	N/A	[30]
SWCNT/PEI	Drop casting	3630	-64	1500	N/A	N/A	[22]
SWCNT/tpp	Vacuum filtration	48	-72	25	0.103	0.078 (310 K)	[31]
SWCNT/dppp	Vacuum filtration	100	-52	27	0.174	0.047 (310 K)	[31]
a-CNT web/BV	N/A	2228	-116	3103	N/A	N/A	[33]
SWCNT/TPM-CB	Drop immersion	497	-59	172	N/A	N/A	[34]
SWCNT/PDINE	Vacuum filtration	500	-47.5	112	N/A	N/A	[36]
SWCNT/NDINE	Vacuum filtration	400	-57	135	N/A	N/A	[36]
SWCNT/CTAB	Vacuum filtration	840	-47	185.7	N/A	N/A	[38]
CNT/KOH/18-crown-6-ether	Drop immersion	2050	-33	230	39	0.002 <sup>a)</sup>	[23]
		69	-63	27	0.124	0.07 <sup>b)</sup>	
s-SWCNT/benzo-18-crown-6-ether	Drop immersion	N/A	N/A	730	1.39	0.12 (298 K)	[39]
CoCp <sub>2</sub> @SWCNT	N/A	432	-41.8	75.4	0.15	0.157 (320 K)	[41]
TDAE-PEDOT/CNT	In situ polymerization	7.3	-1200	1050	0.67	0.5 (room temperature)	[42]
CPE-PyrBlm <sub>4</sub> /SWCNT	N/A	106	-41	17.8	N/A	N/A	[44]

<sup>a)</sup>All TE parameters were measured at an in-plane direction at 310 K; <sup>b)</sup>All TE parameters were measured at a through-plane direction at 310 K.

were converted from p- to n-type, showing  $S$  as high as  $-58 \mu\text{V K}^{-1}$ , presumably due to a process whereby the lone pair of electrons in the nitrogen atoms of PEI were transferred to the nanotubes. However, the value of  $\sigma$  was lowered compared to untreated CNTs because the insulating nature of PEI hinders charge transfer between nanotubes. In response, the same team employed the inorganic reducing agent, NaBH<sub>4</sub>, as the n-type dopant for CNTs due to its strong reducing property.<sup>[27]</sup> It was found that CNTs doped with NaBH<sub>4</sub> showed a lower  $S$  of  $-25 \mu\text{V K}^{-1}$  than that of the PEI treated ones ( $-57 \mu\text{V K}^{-1}$ ). However, a considerably higher  $\sigma$  was obtained in the NaBH<sub>4</sub>-treated samples, but was still below the value of the pristine p-type ones. As a result, to enhance the ultimate TE performance, PEI and NaBH<sub>4</sub> were combined to reduce CNTs to improve the  $S$  to as large as  $-80 \mu\text{V K}^{-1}$  and  $\sigma$  higher than the PEI-doped ones.

As seen from **Figure 1**, the diameters of pristine p-type CNTs (Figure 1a) were relatively smaller than those of n-type counterparts doped with PEI (Figure 1b). Most of the exposed n-type CNTs were coated with a layer of PEI, which is evidenced by the morphology shown in Figure 1a that almost none of the tubular structures were extending from the surface. Considering the electrically insulating coating layers of PEI, the  $\sigma$  of PEI-treated n-type CNTs was greatly reduced. Therefore, DETA, a smaller molecule bearing amine groups similar to PEI, was introduced to examine whether  $\sigma$  can be increased relative to PEI-doped CNTs.<sup>[29]</sup> These efforts showed that the  $S$  value in the DETA-doped CNTs remained positive, indicating that the doping efficiency of DETA is far behind that of PEI. As a

result, by combining large PEI and small DETA dopant molecules, as well as optimizing the mixing ratio of PEI to DETA (67:33 wt%), an  $S$  value of as large as  $-63 \mu\text{V K}^{-1}$  at  $\sigma = 39 \text{ S cm}^{-1}$  was obtained. The  $\sigma$  decreased owing to a significant decrease in carrier mobility from p-type  $\mu_{\text{h}}$  ( $0.365 \text{ cm}^2 \text{ V}^{-1} \text{ s}^{-1}$ ) to n-type  $\mu_{\text{e}}$  ( $0.206 \text{ cm}^2 \text{ V}^{-1} \text{ s}^{-1}$ ). Further reduction with NaBH<sub>4</sub> can improve the PF of the sample to  $38 \mu\text{W m}^{-1} \text{ K}^{-2}$ , which is more than two times higher than the initial n-type analog ( $15 \mu\text{W m}^{-1} \text{ K}^{-2}$ ), as seen in Figure 1c. In order to probe the internal mechanism of the n-type doping processes, the Fermi levels ( $E_{\text{F}}$ s) of the above-mentioned p-type neat CNTs ( $-4.91 \text{ eV}$ ), PEI/DETA-doped samples ( $-4.69 \text{ eV}$ ), and upon reduction with NaBH<sub>4</sub> ( $-4.61 \text{ eV}$ ) were measured. The  $E_{\text{F}}$  values distinctly shifted toward the lowest unoccupied molecular orbital (LUMO) energy level of CNTs ( $-4.59 \text{ eV}$ ), verifying the transition of the p- to n-type.

An injection of reducing agents can further enhance TE performance of n-doped CNTs. For instance, post-treatment of CNTs with reducing agent CaH<sub>2</sub> after DETA doping showed an outstanding  $S$  of  $-41 \mu\text{V K}^{-1}$  and a  $\sigma$  as high as  $165 \text{ S cm}^{-1}$ , reaching a maximum PF of  $27.7 \mu\text{W m}^{-1} \text{ K}^{-2}$ .<sup>[26]</sup> The reduction mechanism of CaH<sub>2</sub> is similar to that of NaBH<sub>4</sub>, which can be explained as follows. Hydride ions are generated from CaH<sub>2</sub> and NaBH<sub>4</sub>. Then,  $2\text{H}^-$  combine to produce hydrogen gas; see Equation (2). The resulting electrons are donated to the nanotubes allowing the transformation from p- to n-type.



**Table 2.** Summary of TE performance of n-type polymer/inorganic nanocrystal TENCs.

TENCs	Preparation method	$\sigma$ [S cm <sup>-1</sup> ]	$S$ [ $\mu$ V K <sup>-1</sup> ]	PF [ $\mu$ W m <sup>-1</sup> K <sup>-2</sup> ]	$\kappa$ [W m <sup>-1</sup> K <sup>-1</sup> ]	$zT$	Ref.
Bi <sub>2</sub> Se <sub>3</sub> /PVDF	Drop casting	51	-80	32.6	0.42	0.02 <sup>a)</sup>	[45]
Cu <sub>0.1</sub> Bi <sub>2</sub> Se <sub>3</sub> /PVDF	Drop casting	146	-84	103.2	0.32	0.1 <sup>a)</sup>	[48]
Ag <sub>2</sub> Te/PVDF	Drop casting	86	-60	30.9	N/A	N/A	[49]
Bi <sub>2</sub> Te <sub>3</sub> /PEDOT:PSS-Glycerol	Spin casting	7.78	-15.7	0.19	N/A	N/A	[50]
Bi <sub>2</sub> Te <sub>3</sub> /PEDOT:PSS	Drop casting	60	-130	80	N/A	N/A	[46]
Bi <sub>2</sub> Te <sub>3</sub> /PEDOT:PSS	Screen printing	73	-137.8	138.6	0.25	0.16 <sup>a)</sup>	[51]
PbTe/PEDOT	Cold pressing	$2 \times 10^{-3}$	-2500	1.44	N/A	N/A	[52]
Bi <sub>2</sub> Te <sub>3</sub> /CF	Unbalanced magnetron sputtering	200	-130	375	0.48	0.38 (473 K)	[53]
WC/PLA	3D printing	50	-11	0.6	0.28	$6.7 \times 10^{-4}$ <sup>a)</sup>	[54]
Ni NWs/PVDF	Drop casting	3100	-27	220	0.55	0.15 (380 K)	[56]
Co NWs/PVDF	Drop casting	6500	-28	523	N/A	N/A	[57]
TiS <sub>2</sub> [(HA) <sub>0.08</sub> (H <sub>2</sub> O) <sub>0.22</sub> (DMSO) <sub>0.03</sub> ]	Electrochemical intercalation	790	-78	450	0.69	0.2 <sup>a)</sup>	[60]
TiS <sub>2</sub> (TBA) <sub>0.013</sub> (HA) <sub>0.019</sub>	Electrochemical intercalation	450	-140	904	1.2	0.23 <sup>a)</sup>	[61]
TiS <sub>2</sub> [(HA)(NMF)] <sup>b)</sup>	Self-assembly	660	-55	210	0.37	0.1 <sup>a)</sup>	[62]
(PANI) <sub>x</sub> V <sub>2</sub> O <sub>5</sub>	Drop immersion	0.1	-30	$9 \times 10^{-3}$	N/A	N/A	[63]
(PEDOT) <sub>0.03</sub> V <sub>2</sub> O <sub>5</sub>	Drop casting	0.16	-350	2	0.68	$10^{-3}$ <sup>a)</sup>	[64]

<sup>a)</sup>All TE parameters were measured at room temperature. <sup>b)</sup>NMF refers to *N*-Methylformamide.

PFs are still at the low or medium level for n-type CNTs doped with insulating organic molecules containing amine groups or reducing agents, not to mention their remarkable air instability. Several feasible methods to improve air stability have been, therefore, implemented in the following studies. Taken as one example, Grunlan and co-workers alternately deposited double walled nanotubes (DWCNTs) and graphene, both of which were stabilized by PEI and polyvinyl pyrrolidone (PVP), respectively, from water using the layer-by-layer (LbL) assembly technique to fabricate n-type TENCs.<sup>[30]</sup> This method generated a highly networked nanocomposite in which well-dispersed DWCNTs and graphene were interconnected between upper and lower layers in the film, thereby significantly improving TE performance of n-type TENCs. A continuous 3D conjugated network, where DWCNTs bridged graphene sheets, provided efficient electron transport paths and increased carrier mobility. The  $S$  value of an 80 bilayered TENC film was also improved due to the energy filtering effect created by the multiple interfaces. Thus the maximum  $\sigma$  of 300 S cm<sup>-1</sup>,  $S$  of -80  $\mu$ V K<sup>-1</sup>, and PF of 190  $\mu$ W m<sup>-1</sup> K<sup>-2</sup> were obtained at room temperature. Interestingly, the graphene platelets in the multilayers seem to act as a barrier to oxygen, thereby increasing air stability. Recently, the Xie group fabricated CNT-based n-type TENCs by dropping PEI solution atop SWCNT films prepared by a floating catalyst chemical vapor deposition method, followed by drying at 50 °C for 5 min (Figure 2a).<sup>[22]</sup> Compared to the above-mentioned fabrication of n-type CNT buckypaper with PEI dopant through ultrasonication and doping process illustrated in Figure 2b, this method showed superior TE performance. In particular, these TENCs showed a much higher  $\sigma$  due to the absence of the weak and blocked CNT junctions caused by the insulating polymer, which would adversely influence carrier transport between nanotubes. A very attractive PF of 1500  $\mu$ W m<sup>-1</sup> K<sup>-2</sup> was thus

obtained by doping with 1 wt% PEI solution in ethanol. Furthermore, the resulting n-type films showed excellent ambient stability with both  $S$  and  $\sigma$  maintaining over 95% of the initial value after 3 months.

A variety of other n-type dopants have also allowed for the effective transfer of electrons to CNTs. Given that phosphorus is in the same main group of the periodic table as nitrogen, phosphine-containing organic molecules may provide interesting alternatives. Indeed, an early study introduced several phosphine-containing aromatic molecules, including 1,3-bis(diphenylphosphino)propane (dppp), triphenylphosphine (tpp), and bis[(diphenylphosphinomethyl)phenylphosphino]methane (dpmppm), whose chemical structures are given in Scheme 1.<sup>[31]</sup> As predicted, SWCNTs treated with these P-based dopants exhibited n-type characteristics, in particular the PFs of tpp- and dppp-doped samples surpassed 25  $\mu$ W m<sup>-1</sup> K<sup>-2</sup>, more than 2.5 times higher than that of similar PEI-doped analogs. The TE performance as a function of tpp concentration was measured to elucidate the n-doping mechanism. As seen in Figure 3a, an increasing tpp concentration leads to a decrease of  $S$  while  $\sigma$  initially decreases and then increases gradually. This phenomenon can be ascribed to decreasing hole concentrations in the valence band (VB) and an increase of electron densities in the conduction band (CB). In this regard, the CNTs were p-type doped with oxygen impurity which could inject holes into the VB or trap thermally activated electrons on the CB. At the low doping level, electrons from the tpp dopant would offset the holes in the CNTs, which led to a decrease of both  $S$  and  $\sigma$ ; in contrast, in the case of heavy doping, electron carriers were injected into the CNTs so that both  $S$  and  $\sigma$  increased, as illustrated in Figure 3b.

Several viologens were used as n-type dopants via direct redox reaction or charge transfer.<sup>[32]</sup> It is worth recalling that

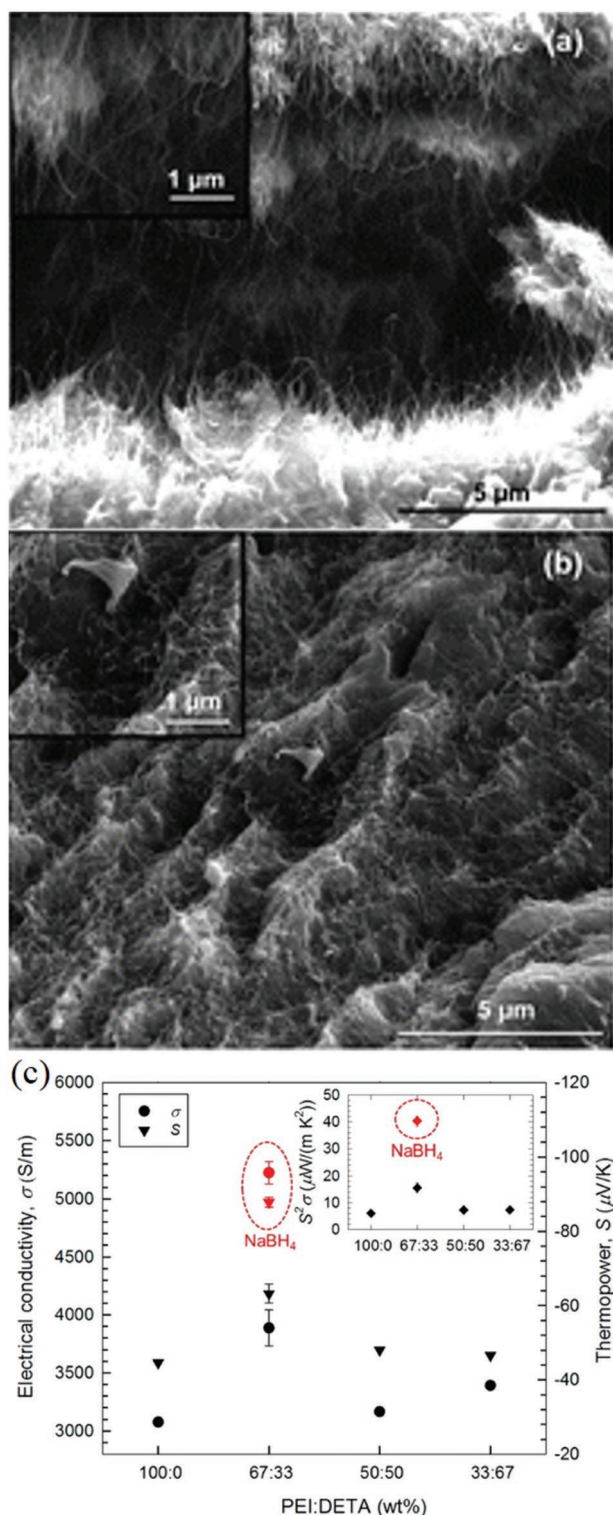


**Figure 1.** Cross-sectional scanning electron microscopy (SEM) image of a) pristine p-type CNTs and b) n-type CNTs doped with PEI. a,b) Reproduced with permission.<sup>[27]</sup> Copyright 2012, The Royal Society of Chemistry. c) The measured  $\sigma$  (circle) and  $S$  (triangle) values of the n-type CNT samples doped with different PEI to DETA weight ratios as well as the PFs (rhombus) are shown in the inset. The sample within the red dashed circles refers to a film doped with a PEI:DETA ratio of 67:33 and further reduced by NaBH<sub>4</sub>. Reproduced with permission.<sup>[29]</sup> Copyright 2014, The American Chemical Society.

there exist three different oxidation states for typical viologens with distinct colors including yellow/brown/red neutral V<sup>0</sup> (colors depending on the concentration), violet V<sup>•+</sup>, and colorless V<sup>2+</sup> as shown in Figure 4b. As seen in Figure 4a, the colorless viologen molecules (V<sup>2+</sup>) were first dissolved in water. After adding NaBH<sub>4</sub>, V<sup>2+</sup> was reduced to V<sup>•+</sup> and further transformed to neutral V<sup>0</sup> followed by spreading into nonpolar solvent toluene. Viologen (V<sup>0</sup>) possesses a relatively low reduction potential so that it acted as a strong reducing agent. Thus, the neutral viologen molecules tended to be transformed to V<sup>2+</sup> spontaneously by transferring electrons to CNTs. As a proof of-concept, 1,1'-dibenzyl-4,4'-bipyridinium dichloride (BV), see Scheme 1, was introduced as an n-type CNT dopant. Moreover, BV-doped CNTs showed outstanding long-term stability under ambient conditions, as well as water stability, presumably due to the hydrophobic property of the V<sup>0</sup> protecting layer. Moreover, oxygen desorption by thermal treatment was introduced to improve the n-type doping efficiency owing to the removal of n-type doping sites on CNTs as occupied by oxygen.<sup>[33]</sup> As a result, a BV-treated annealed CNT (namely a-CNT) web showed a PF as high as 3103  $\mu\text{W m}^{-1} \text{K}^{-2}$  compared to that of the BV-treated pristine CNT web (1901  $\mu\text{W m}^{-1} \text{K}^{-2}$ ). A similar phenomenon was also observed for other dopants such as PEI and tpp. The air stability of the BV-doped a-CNT web was superior to that of the PEI-doped counterparts, suggesting that BV can effectively wrap CNTs and retard reactions with oxygen.

Malachite green (MG) (Scheme 1) can exist in different forms by manipulating the pH of the aqueous solution.<sup>[34]</sup> At a pH value higher than 11.6, MG hydrochloric acid salts would transform into two dimethylamine units containing triphenylmethane (TPM)-CB, which showed more efficient n-type doping for CNTs than MG. TPM-CB nanoparticles gradually formed when the pH reached 12 and produced SWCNT/TPM-CB TENC films. These materials showed an  $S$  of  $-59 \mu\text{V K}^{-1}$  and a  $\sigma$  as high as  $497 \text{ S cm}^{-1}$ , which is similar to the conductivity of pristine SWCNTs. Excellent stability was also reported, which was attributed to the partial resonant quinoidal structure of the cationic form of TPM-CB caused by the electron transfer to SWCNTs.

Another means of fabricating n-type CNT-based TENCs is to combine CNTs with organic semiconductors, which can enhance TE performance due to the intrinsic high  $\sigma$  compared to that of the insulating dopants. For example, rylene diimides have been widely used in the fabrication of n-channel field-effect transistors and organic p-n junctions because of their high electron affinities, air stability, and solution processing.<sup>[35]</sup> Thus, amino-substituted rylene derivatives of perylene diimide (PDINE) and naphthalene diimide (NDINE) were included to prepare TENCs.<sup>[36]</sup> Owing to the strong  $\pi$ - $\pi$  interfacial interactions between the crystal PDINE (or NDINE) and CNTs, the interconnected SWCNT network wrapped the crystals and well-dispersed blends were formed. Only a very short time of 0.5 h was needed to dope the SWCNTs with PDINE and NDINE, compared with doping times as long as 48 h when using PEI. Ultimately, maximum PFs of 112 and 135  $\mu\text{W m}^{-1} \text{K}^{-2}$  were achieved for the optimized PDINE/SWCNT and NDINE/SWCNT, respectively. Besides, the air stability and thermal stability of both composites are superior to those of PEI/SWCNT, which began to lose weight even at 40 °C.<sup>[23]</sup>

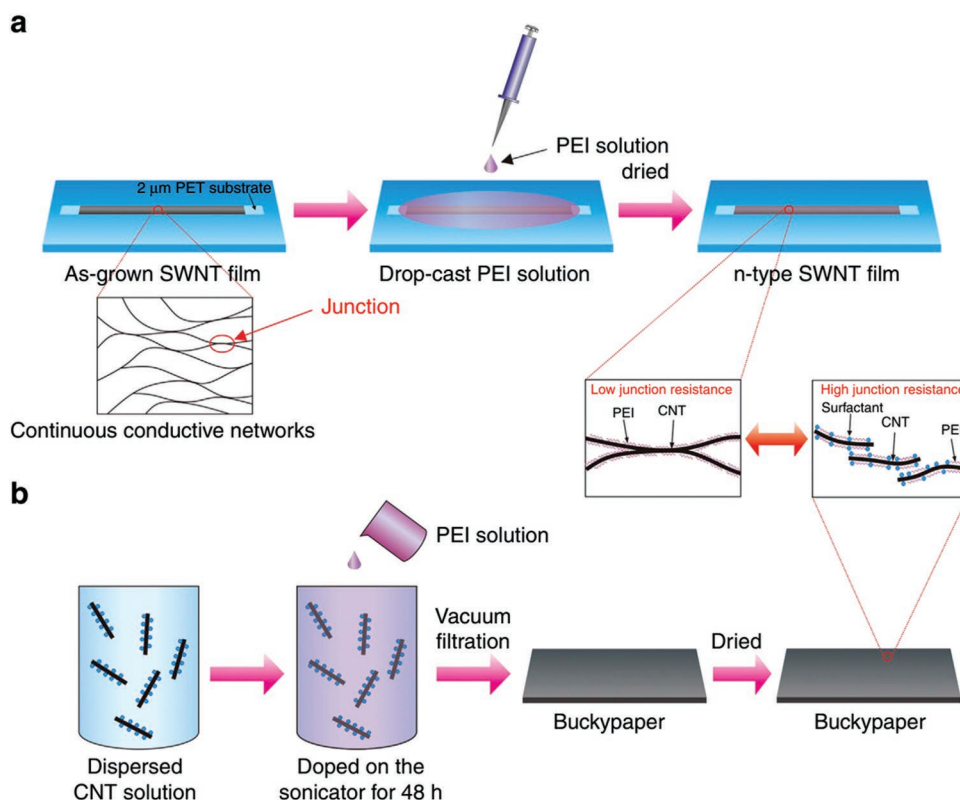
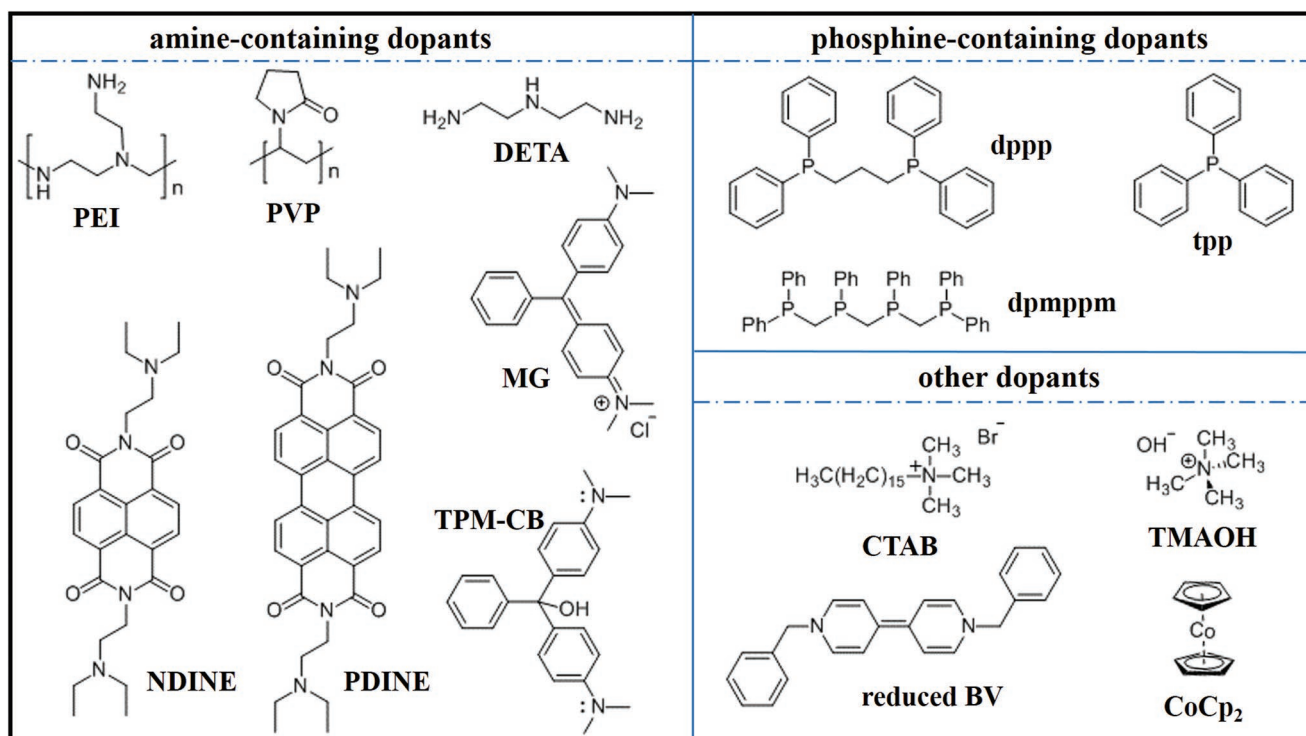


**Figure 2.** Schematics of different fabrication processes used for preparing n-type PEI-doped CNT-based flexible films. a) n-Type SWCNT films based on SWCNT continuous networks synthesized by the floating catalyst chemical vapor deposition method. b) n-type CNT buckypapers based on dispersed CNT solutions. All panels reproduced with permission.<sup>[22]</sup> Copyright 2017, Nature Publishing Group.



**Scheme 1.** Chemical structures of molecular dopants used for the preparation of n-doped CNTs.

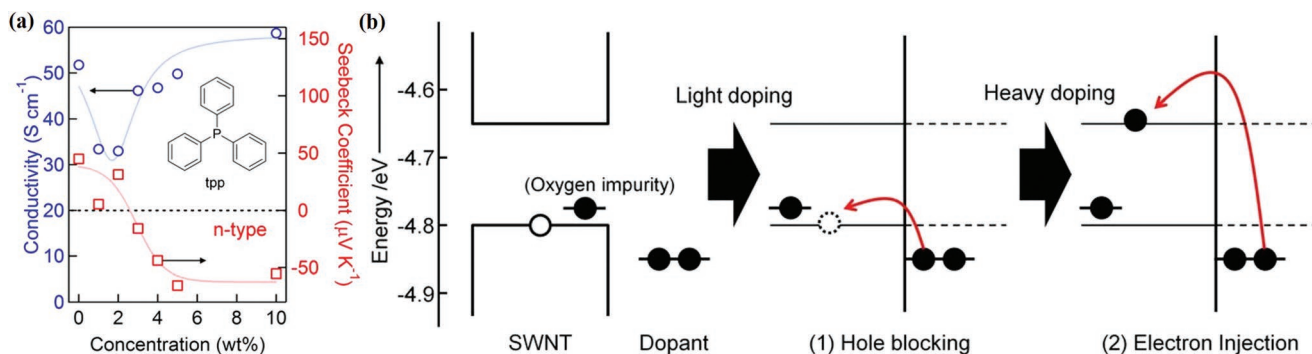


**Figure 3.** a) The relationship between  $\sigma$  (blue),  $S$  (red), and doping level of tpp-doped SWCNTs, which was fixed by the dopant concentration of the tpp solutions. b) A possible explanation for n-type doping mechanism. a,b) Reproduced with permission.<sup>[31]</sup> Copyright 2013, Nature Publishing Group.

Anions of ammonium salts have proven to be effective in n-doping  $\pi$ -acidic [6,6]-phenyl-C61-butyric methyl ester (PC<sub>61</sub>BM) through an anion-induced electron transfer process.<sup>[37]</sup> Based on the above precedent, different kinds of tetraalkylammonium salts were exploited as n-type dopants of CNTs. For instance, Kawai and co-workers<sup>[23]</sup> used tetramethylammonium hydroxide (TMAOH) (Scheme 1) in aprotic solvents such as *N*-methyl pyrrolidone (NMP) and *N,N*-dimethylformamide (DMF) to treat SWCNTs and reported excellent TE performance. The hydroxide ion (OH<sup>-</sup>) is commonly thought to be a weak reductant in protic solvents; however, this is not the case in aprotic solvents, so that the electron-donating ability of OH<sup>-</sup> would be able to n-dope CNTs. Likewise, the commonly used surfactant cetyltrimethylammonium bromide (CTAB) (Scheme 1) was introduced to n-type doped CNTs.<sup>[38]</sup> An outstanding PF of 185.7  $\mu\text{W m}^{-1} \text{K}^{-2}$  was obtained at an SWCNT:

CTAB ratio of 10: 5 (w/w) in DMF solvent, which would contribute to the n-type doping of SWCNT to some extent. The influences of anion type and alkyl chain of the surfactant on TE performance were also taken into account. It was found that the  $\sigma$  of n-type SWCNT doped by surfactants with different halide anions was very close in value, yet the  $S$  of iodine-containing samples was significantly lower than that of the chlorine and bromine ones, indicating a lower doping efficiency of I<sup>-</sup> compared to Cl<sup>-</sup> and Br<sup>-</sup>. The alkyl chain length had a negligible effect on the TE performance. Moreover, these nonreactive salts with alkali-metal cations and hydroxide or halide anions such as KCl and NaOH were combined with crown ethers to n-doped CNTs, as shown in Figure 5a.<sup>[23]</sup> Crown ether and metal ion complexes ([M-crown]<sup>+</sup>) were formed, while the halide anions formed halogen molecules and donated electrons to CNTs (halogen molecules were removed by post-treatment). This hypothesis could be verified by the evidence that n-type CNTs contained considerable metal ions with almost no halogen through energy dispersive X-ray spectroscopy (EDS) measurements. More importantly, as shown in Figure 5b, SWCNT films treated with mixed KOH and benzo-18-crown-6-ether exhibited surprisingly good air stability, for which no obvious decrease of PF was observed even after 1 month at 100 °C. This outstanding property was explained by the hard-soft-acid-base (HSAB) principle—the soft-acid coordination of [M-crown]<sup>+</sup> was stabilized by the soft base, i.e., negatively charged SWCNT. The same mixed dopants were also used to dope semiconducting single-walled carbon nanotubes (s-SWCNTs) and a PF of 730  $\mu\text{W m}^{-1} \text{K}^{-2}$  was achieved.<sup>[39]</sup> To overcome the extreme air instability of n-type s-SWCNTs, Al<sub>2</sub>O<sub>3</sub> was added as a protection layer by using the atomic layer deposition (ALD) method. The resulting film presented excellent stability in air with a decrease of  $S$ ,  $\sigma$ , and PF less than 5% for almost half a month.

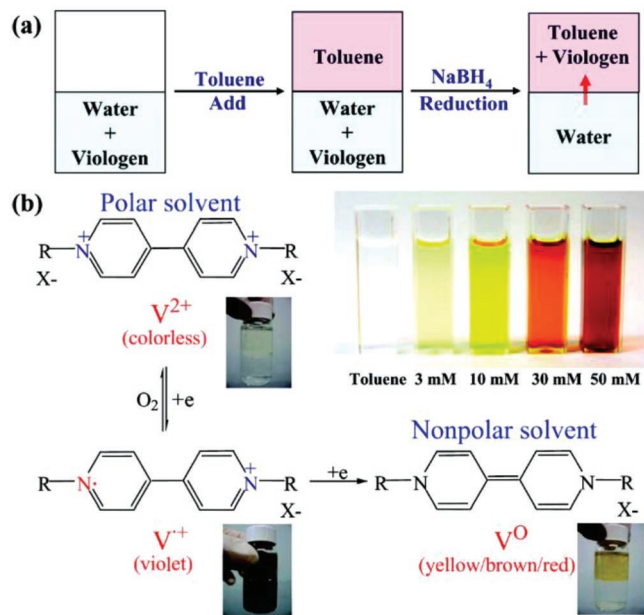


**Figure 4.** a) The preparation procedure of reducing viologen agent in two solvent systems. b) Three different oxidation states of viologens with distinct colors and the color dependence on the reduced viologen concentration. a,b) Reproduced with permission.<sup>[32]</sup> Copyright 2009, The American Chemical Society.

All of the work described above on n-type TENCs, regardless of the doping mechanisms, has been realized by adsorbing dopant molecules on the outer surfaces of CNTs. Alternately, several studies have focused their attention on the encapsulation of dopants inside the inner spaces of the CNTs, which would not affect the electrical conductivity of CNTs yet might improve TE performance. For instance, cobaltocene (CoCp<sub>2</sub>)-encapsulated SWCNTs (CoCp<sub>2</sub>@SWCNTs) were prepared, and their n-type characteristics were confirmed by the negative value of  $S$  ( $-41.8 \mu\text{V K}^{-1}$  at 320 K).<sup>[40]</sup> X-ray photoelectron spectroscopy

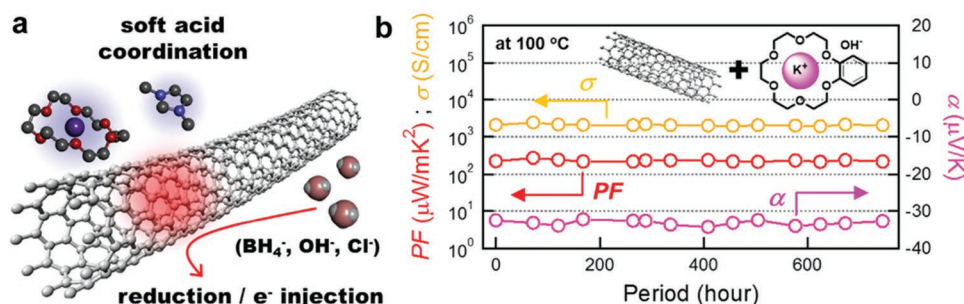


**Figure 5.** a) Schematic concept of salt and crown ether-induced n-type doping. b) Air stability of the  $\sigma$  (yellow),  $S$  (purple), and PF (red) of n-type CNTs treated with KOH/benzo-18-crown-6-ether at 100 °C. a,b) Reproduced with permission.<sup>[23]</sup> Copyright 2016, Wiley-VCH.

(XPS) measurements revealed that the oxidation state of almost all the Co atoms was Co<sup>3+</sup> instead of Co<sup>2+</sup>, indicating the formation of cobaltocenium and electron transfer from CoCp<sub>2</sub> to SWCNTs.<sup>[41]</sup> The resulting  $\sigma$  of the CoCp<sub>2</sub>@SWCNTs film was 432 S cm<sup>-1</sup>, almost ten times higher than pristine SWCNTs. This feature can be interpreted by the increased carrier density caused by the doping process. Ultimately, a  $zT$  value of 0.157 was obtained at 320 K together with excellent air stability and great flexibility.

## 2.2. Blends of n-Type Polymers and CNTs

To fabricate n-type CNT-based TENCs, Yu and co-workers utilized an in situ polymerization method to synthesize poly(3,4-ethylenedioxythiophene) (PEDOT)/CNT by using FeCl<sub>3</sub> oxidant.<sup>[42]</sup> The resulting p-type PEDOT was transformed to n-type by doping with tetrakis(dimethylamino)ethylene (TDAE). CNTs were also n-type doped through the TDAE treatment, as evidenced by the shift of work function toward the vacuum level. An ultrahigh PF up to 1050  $\mu\text{W m}^{-1} \text{K}^{-2}$  was obtained at 10.7 wt% CNT owing to a surprisingly high  $S$  ( $-1200 \mu\text{V K}^{-1}$ ), which was caused by a greatly decreased carrier concentration and partially percolated CNT networks, and a moderate  $\sigma$  due to the almost unchanged high mobility of CNTs.

Bazan and co-workers employed n-type conjugated polyelectrolytes (CPEs) to formulate TENCs.<sup>[43,44]</sup> It is worth noting that CPEs can help CNTs disperse in polar solvents due to their hydrophobic backbone and pendant ionic functionalities. According to whether anionic or cationic side groups are attached to the same backbone, the CPEs can be broadly classified into p- or n-type, respectively. Two CPEs with the same cationic groups comprising pyridinium (PyrBIm<sub>4</sub>) and different conjugated backbones, namely poly(fluorene-*alt*-benzothiadiazole) (PFBT) and poly(cyclopenta-[2,1-*b*;3,4-*b'*]-dithiophene-*alt*-4,7-(2,1,3-benzothiadiazole)) (CPDT-*alt*-BT) (Figure 6a), were chosen to be blended with SWCNTs. These two TENCs were denoted as PFBT-PyrBIm<sub>4</sub>/SWCNT and CPE-PyrBIm<sub>4</sub>/SWCNT, respectively. CPE-PyrBIm<sub>4</sub> showed better n-type doping efficiency than PFBT-PyrBIm<sub>4</sub> because CPE-PyrBIm<sub>4</sub>/SWCNT composites converted to p-type at a high CNT content, while the PFBT-containing ones exhibited p-type at medium CNT loading. With increasing SWCNT contents in the TENC films,  $\sigma$  increased progressively in PFBT-PyrBIm<sub>4</sub>/SWCNT, while CPE-PyrBIm<sub>4</sub>/SWCNT displayed a maximum

value at 1:1 wt%, as shown in Figure 6b,c. In the 2:3 blend of CPE-PyrBIm<sub>4</sub> and SWCNT, the conventional p-doping of the SWCNT was no longer compensated by n-type doping by the cationic CPEs, leading to a lower effective charge carrier density and a smaller  $\sigma$ . The highest PF obtained for n-type CPE-PyrBIm<sub>4</sub>/SWCNT composite was 17.8  $\mu\text{W m}^{-1} \text{K}^{-2}$  at a mass ratio of 1:1.

## 3. Organic:Inorganic Nanocrystal Blends

Owing to a superior TE performance relative to their organic counterparts, inorganic nanocrystals are also often used as fillers in TENCs. Hybridization of polymers with inorganic nanostructures not only can yield solution-processable and flexible TENCs but also achieve better TE performance than organic materials due to synergistic effects between both components. For instance, traditional inorganic TE materials—Bi<sub>2</sub>Se<sub>3</sub> and PbTe—possess  $\kappa$  of 1.1–2.1 W m<sup>-1</sup> K<sup>-1</sup>, almost one order of magnitude higher than most organic materials;<sup>[45,46]</sup> yet, the  $\kappa$  in TENCs is greatly reduced due to the presence of heterointerfaces within the nanocomposites that scatter thermal phonons. Another favorable consequence is the energy-filtering effect of charge carriers. Energetic mismatches at inorganic/organic interfaces can selectively scatter low-energy carriers, resulting in an increased average energy of the carriers in the TENCs, which significantly enhances the  $S$ .<sup>[47]</sup> A rational engineering of the inorganic/organic interfaces through deeper knowledge of the underlying mechanisms is therefore a promising way to achieve high-performance TENCs.

### 3.1. Blends with Semiconductor NCs

Inorganic semiconductor nanocrystals, such as Bi<sub>2</sub>Te<sub>3</sub> and Ag<sub>2</sub>Te, are usually blended with polymers. The resulting TENCs have received increased attention due to their potential low-cost solution-processing methods, such as drop-casting and spin-coating, and better TE performance when compared to pure organic materials. The polymer matrices, inorganic nanostructures, the size and dispersion of inorganic nanostructures, and the preparation methods ultimately modify the TE performance of TENCs.

Polyvinylidene fluoride (PVDF) has been considered as a particularly useful matrix for TENCs owing to its low cost,

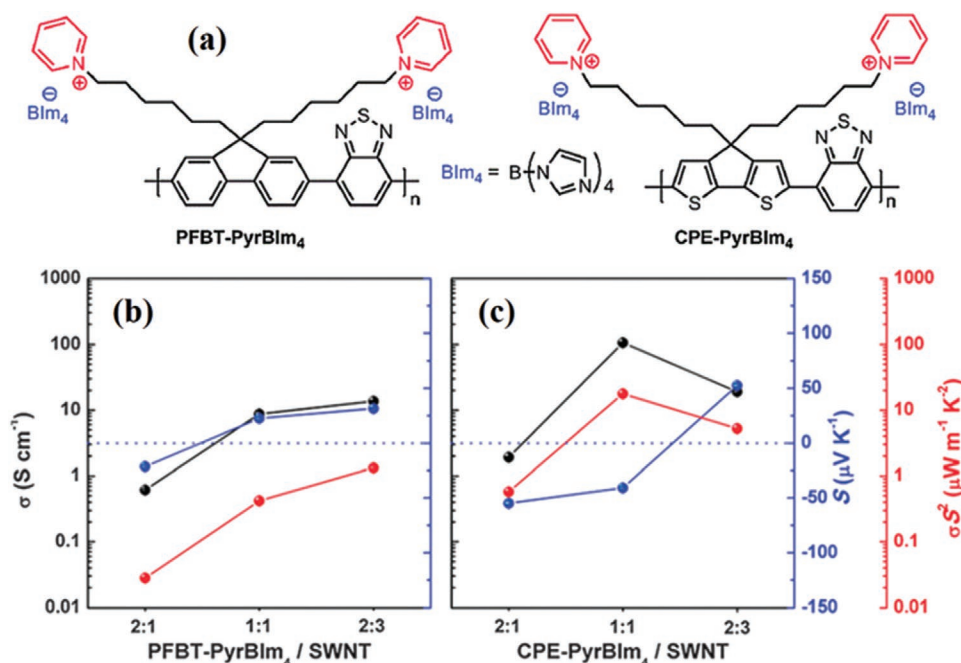


**Figure 6.** a) Chemical structures of two cationic CPEs. Dependence of  $\sigma$  (black),  $S$  (blue), and PF (red) on different weight ratios for b) PFBT-PyrBlm<sub>4</sub>/SWCNT and c) CPE-PyrBlm<sub>4</sub>/SWCNT TENCs. All panels reproduced with permission.<sup>[44]</sup> Copyright 2015, The Royal Society of Chemistry.

superior flexibility, excellent thermal/chemical stability, and ultralow thermal conductivity. PVDF can also endow solution-processed n-type TENCs with good durability and even protect the inorganic nanostructures from degradation of TE performance caused by oxidation.

For example, a highly flexible and free-standing n-type TE fabric based on layered Bi<sub>2</sub>Se<sub>3</sub> nanoplates (NPs) and PVDF was fabricated by the Carroll group simply through drop-casting followed by peeling off from the substrate.<sup>[45]</sup> The optimal system exhibited  $S$  and  $\sigma$  values of  $-80 \mu\text{V K}^{-1}$  and  $51 \text{ S cm}^{-1}$  at room temperature, respectively, both of which are lower than those of bulk Bi<sub>2</sub>Se<sub>3</sub>. However, the  $\kappa$  of the TENCs was reduced from 1.1 to  $0.42 \text{ W m}^{-1} \text{ K}^{-1}$  at 300 K as expected, a feature that was attributed to phonon scattering by grain boundaries between the platelets and the embedded PVDF. Finally, the optimal  $zT$  value reached 0.02, nearly the same as that of bulk Bi<sub>2</sub>Se<sub>3</sub>. Such PVDF-based TENC fabrics were verified with excellent flexibility by bending tests which showed that the PF maintained 85% of the initial value after 1500 bends. The PF of the fabrics could be significantly improved to achieve higher  $zT$  by optimizing the TE performance of Bi<sub>2</sub>Se<sub>3</sub> NPs. Specifically, the same group used Cu atoms to dope Bi<sub>2</sub>Se<sub>3</sub> NPs by a one-step solution growth method and prepared Cu<sub>x</sub>Bi<sub>2</sub>Se<sub>3</sub>/PVDF TENC fabrics by using the same drop-casting method.<sup>[48]</sup> Figure 7a,b show the TE performance of TENC films with different Cu doping concentrations. A PF as high as  $103 \mu\text{W m}^{-1} \text{ K}^{-2}$  was realized with the Cu<sub>0.1</sub>Bi<sub>2</sub>Se<sub>3</sub> NPs/PVDF TENCs, which is about 3.5 times in comparison to the Bi<sub>2</sub>Se<sub>3</sub> NPs/PVDF, leading to the optimal  $zT$  value of 0.1. The significantly enhanced PF not only resulted from the improvement of TE performance of Bi<sub>2</sub>Se<sub>3</sub> NPs, but also from the decoupling of  $\sigma$  and  $S$  during the Cu-doping process (Figure 7a,b), which was ascribed to the filtration of low-energy electrons at the Cu<sub>x</sub>Bi<sub>2</sub>Se<sub>3</sub>/PVDF interfaces. As

illustrated in Figure 7c,d, PVDF created interfacial energy barriers ( $E_b$ ) between Cu<sub>x</sub>Bi<sub>2</sub>Se<sub>3</sub> NPs, and only those carriers with energies higher than  $E_b$  could pass through and contribute to the ultimate enhancement of  $S$ . Shi and co-workers prepared a flexible and robust n-type TE fabrics based on Ag<sub>2</sub>Te nanoshuttles and PVDF using a solution-processable method without the need for a surfactant.<sup>[49]</sup> A decoupling effect between the interrelated  $\sigma$  and  $S$  was also observed owing to the energy barrier filtering effect introduced by the Ag<sub>2</sub>Te/PVDF junctions, which led to a maximum PF of  $30.9 \mu\text{W m}^{-1} \text{ K}^{-2}$ . The estimated  $\kappa$  value was  $0.4 \text{ W m}^{-1} \text{ K}^{-1}$  without considering the existence of PVDF and plentiful grain boundaries. Thus, the real  $zT$  for Ag<sub>2</sub>Te nanoshuttle/PVDF TENC films could be much greater than 0.02 at 300 K.

Another frequently used choice for TENC matrix is the conducting polymer PEDOT. For commercially available Clevios PH1000, a high PF of  $\approx 47 \mu\text{W m}^{-1} \text{ K}^{-2}$  with  $\sigma = 945 \text{ S cm}^{-1}$  and  $S = 22 \mu\text{V K}^{-1}$  was achieved.<sup>[46]</sup> The high  $\sigma$  and low  $\kappa$  of poly(3,4-ethylenedioxythiophene):polystyrene sulfonate (PEDOT:PSS) make it an appealing partner for blending with inorganic NCs. For example, the Umar group reported the fabrication of p-type and n-type Bi<sub>2</sub>Te<sub>3</sub>/PEDOT:PSS-glycerol TENC films by using a simple mixing and drop-casting approach.<sup>[50]</sup> The optimum  $\sigma$  and  $S$  of the n-type samples were  $7.78 \text{ S cm}^{-1}$  and  $-15.7 \mu\text{V K}^{-1}$ , respectively. Considering that the main charge carriers of PEDOT were holes, a part of the  $S$  of n-type Bi<sub>2</sub>Te<sub>3</sub> was canceled. Furthermore, the Katz group prepared p-type and n-type Bi<sub>2</sub>Te<sub>3</sub>/PEDOT:PSS (Clevios PH1000) TENC fabrics with a bilayer structure by successively drop-casting Bi<sub>2</sub>Te<sub>3</sub> solution and PEDOT:PSS emulsion on a glass slide.<sup>[46]</sup> Bilayer structures were observed in both cross-sectional and top view scanning electron microscopy (SEM) images of the as-prepared Bi<sub>2</sub>Te<sub>3</sub>/PEDOT:PSS TENCs (Figure 8). Interestingly, a volume fraction

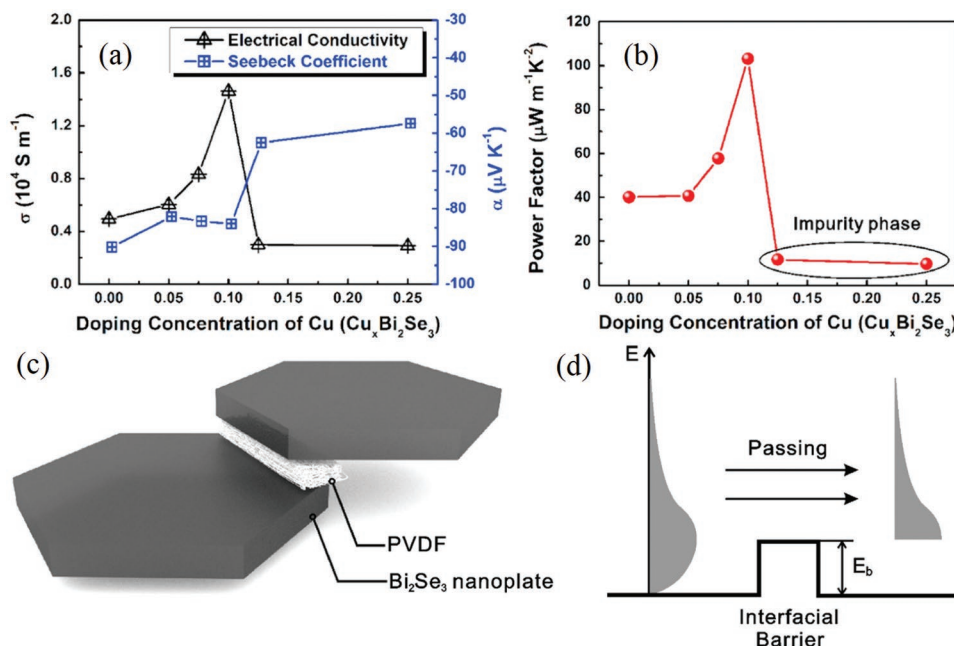


**Figure 7.** a) The  $\sigma$  and  $S$  of the  $\text{Cu}_x\text{Bi}_2\text{Se}_3$ /PVDF TENC fabrics with different Cu-doping concentrations at 300 K. b) The PFs of  $\text{Cu}_x\text{Bi}_2\text{Se}_3$ /PVDF TENC fabrics with different Cu-doping concentrations at 300 K. c) Illustration of the energy barrier between PVDF two  $\text{Bi}_2\text{Se}_3$  NPs. d) Illustration of the impact of the interfacial barrier. All panels reproduced with permission.<sup>[48]</sup> Copyright 2015, Elsevier.

of 10% p-type PEDOT:PSS in the TENCs did not decrease the  $S$  of the n-type  $\text{Bi}_2\text{Te}_3$  particles. The PF was obtained as  $80 \mu\text{W m}^{-1} \text{K}^{-2}$  at this volume ratio. A similar bilayer strategy was used by We et al.<sup>[51]</sup> To fabricate flexible hybrid films, they screen-printed an n-type  $\text{Bi}_2\text{Te}_3$  inorganic film followed by infiltrating with PEDOT:PSS solutions. Compared with the pure  $\text{Bi}_2\text{Te}_3$  inorganic film, both the  $\sigma$  and  $\kappa$  of the optimal TENC films increased while  $S$  just slightly decreased, which was attributed to the  $\approx 9\%$  increase in carrier concentration. As a result, a  $zT$  value of the n-type hybrid film as high as 0.16 was achieved at 300 K, slightly higher than that of the neat  $\text{Bi}_2\text{Te}_3$  film.

Different from the generally applied PEDOT:PSS, the majority carriers turned to be electrons when PEDOT was dedoped, which presented a high negative  $S$ . Cai and co-workers prepared PbTe-modified PEDOT nanotubes at room temperature by an in situ interfacial polymerization method.<sup>[52]</sup> The morphology of PbTe-modified PEDOT nanotubes was imaged

by transmission electron microscopy (TEM) (Figure 9b,b'). The dedoped PEDOT exhibited n-type characteristics and showed a high  $S$  of  $-4088 \mu\text{V K}^{-1}$ , which is due to the dedoping of the PEDOT nanotubes by removing the counterions ( $\text{Cl}^-$ ) during the fabrication process. When the PbTe content was increased from 0 to 44 wt%, the  $\sigma$  of the cold-pressed pellets increased to  $0.616 \text{ S m}^{-1}$ , while the absolute  $S$  value decreased from 4088 to  $1205 \mu\text{V K}^{-1}$  (Figure 9a), indicating that the TE performance of PEDOT nanotubes can be tuned by adjusting the PbTe concentration.

Apart from PVDF and PEDOT, other polymers used to construct n-type TENCs include cellulose fibers (CFs) and polylactic acid (PLA). Tai and co-workers developed a novel strategy to make hybrid  $\text{Bi}_2\text{Te}_3$  thick films with CFs through an unbalanced magnetron sputtering technique, where the CFs served as a hierarchical porous template.<sup>[53]</sup> The  $\kappa$  was greatly lower than those of the bulk  $\text{Bi}_2\text{Te}_3$  because all phonons could be

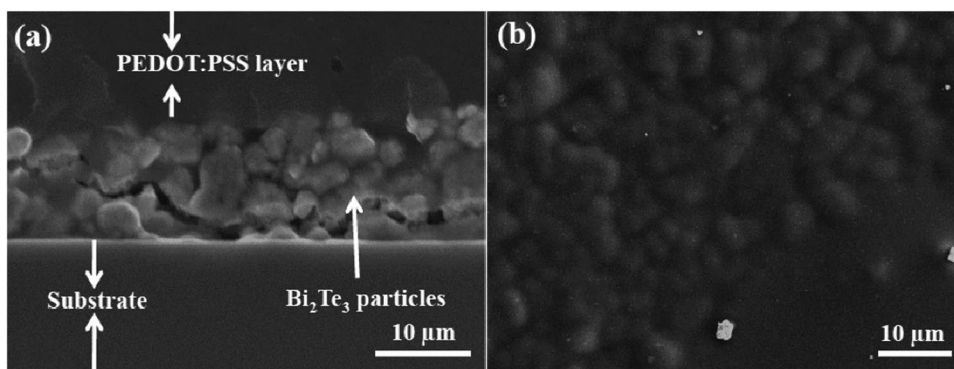


**Figure 8.** a) Cross-sectional and b) top view SEM images of ball-milled  $\text{Bi}_2\text{Te}_3$  particles infiltrated with PH1000. a,b) Reproduced with permission.<sup>[46]</sup> Copyright 2010, The American Chemical Society.

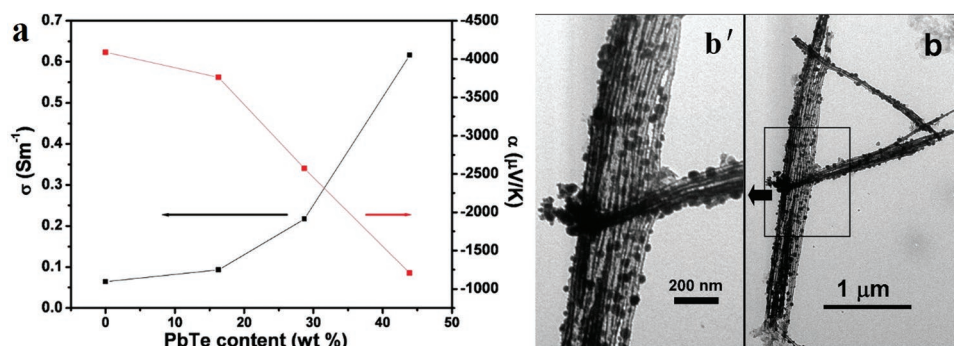


**Figure 9.** a) The  $\sigma$  and  $S$  (here shown as  $\alpha$ ) of the composite pellets as a function of PbTe content. TEM pictures of the b) PbTe-modified PEDOT nanotube sample, and b') high-magnification picture of the marked area in panel (b). a,b) Reproduced with permission.<sup>[52]</sup> Copyright 2011, The American Chemical Society.

strongly scattered by nano/microscale hierarchical pores (Figure 10). Meanwhile,  $S$  was increased because of the interfacial barrier scattering between Bi<sub>2</sub>Te<sub>3</sub> and the thin Bi<sub>2</sub>Te<sub>3</sub> oxidation layer. As a result, the  $zT$  value as high as 0.38 was obtained at 473 K. In addition, Du et al. prepared n-type tungsten carbide (WC)/PLA TENC films by 3D printing.<sup>[54]</sup> The highest  $zT$  value of as prepared WC/PLA TENCs was about  $6.7 \times 10^{-4}$  at 300 K. Compared with the conventional high-energy-consumption methods, such as solution mixing and in situ polymerization, 3D printing could largely save both materials and time, making it possible to fabricate TENCs with complex geometric configurations.<sup>[55]</sup>

### 3.2. Blends with Metallic Nanostructures

Despite their intrinsic high electrical conductivity and low cost, metals have been seldom reported as the inorganic component of TENCs, especially n-type. We demonstrated for the first time that blends of a metal and an insulating polymer, both of which were poor TE materials due to their high thermal conductivity and poor electrical properties, respectively, could be brought together to construct a nanocomposite exhibiting excellent TE performance.<sup>[56]</sup> This effort led to the dopant-free solution fabrication of highly bendable n-type TENCs

comprising metallic Ni nanowires (NWs) embedded in an insulating PVDF matrix. The  $\sigma$  and  $S$  of these TENCs were decoupled and both increased with Ni content (Figure 11a). 3D percolation networks gradually formed in the process, leading to the highest PF of  $200 \mu\text{W m}^{-1} \text{K}^{-2}$  at 80 wt% Ni content (Figure 11b). These TENCs also showed the typical temperature dependence of Ni, specifically, negative in  $\sigma$ , while positive in absolute  $S$ . Moreover, a remarkably low thermal conductivity of  $0.55 \text{ W m}^{-1} \text{K}^{-1}$  was found in these TENCs. Thus, the maximum PF of  $220 \mu\text{W m}^{-1} \text{K}^{-2}$  and the best  $zT$  of 0.15 were obtained at 380 K with 80 wt% (44.5 vol%) Ni NWs.

In the above-mentioned study, precise control of the morphology directly relevant to TE performance was absent, so that the Ni NWs were randomly distributed within the PVDF matrix. To resolve this issue, we further provided a facile strategy to improve the blend film morphology of n-type TENCs consisting of polymer and inorganic metallic nanofillers.<sup>[57]</sup> As a proof of concept, we utilized the magnetic characteristics of Co NWs to direct the assembly of metallic nanowires within the PVDF matrix through a solution fabrication method, which would significantly enhance the  $\sigma$  of TENCs, as illustrated in Figure 11c,d. The resulting oriented n-type TENCs, which are shown in the SEM image Figure 11f, exhibited significantly increased  $\sigma$  in comparison to randomly packed nanocomposites (Figure 11e). As a result, the maximum PF of  $523 \mu\text{W m}^{-1} \text{K}^{-2}$

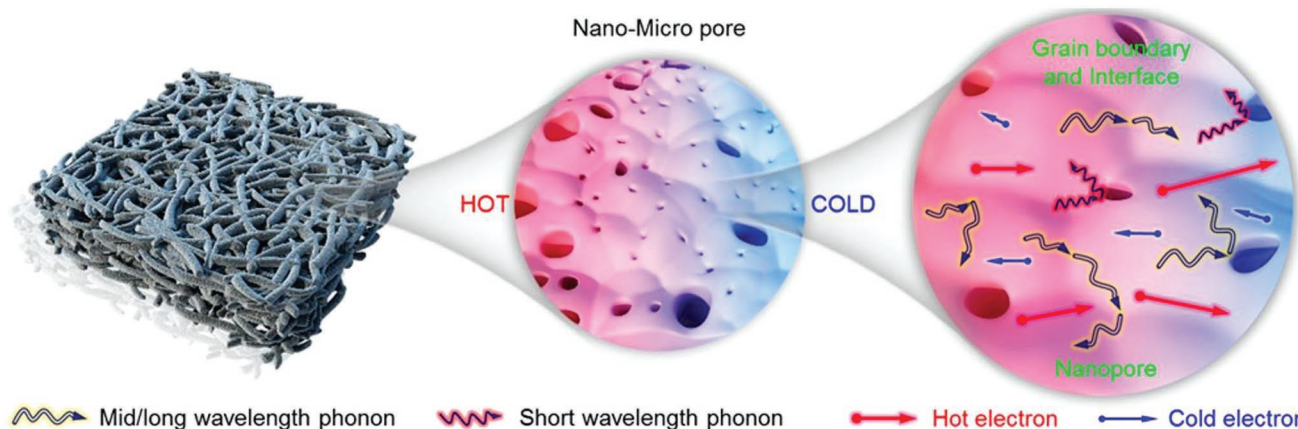


**Figure 10.** Schematic diagram of flexible TE materials with nano/microscale hierarchical pores. Reproduced with permission.<sup>[53]</sup> Copyright 2018, The American Chemical Society.

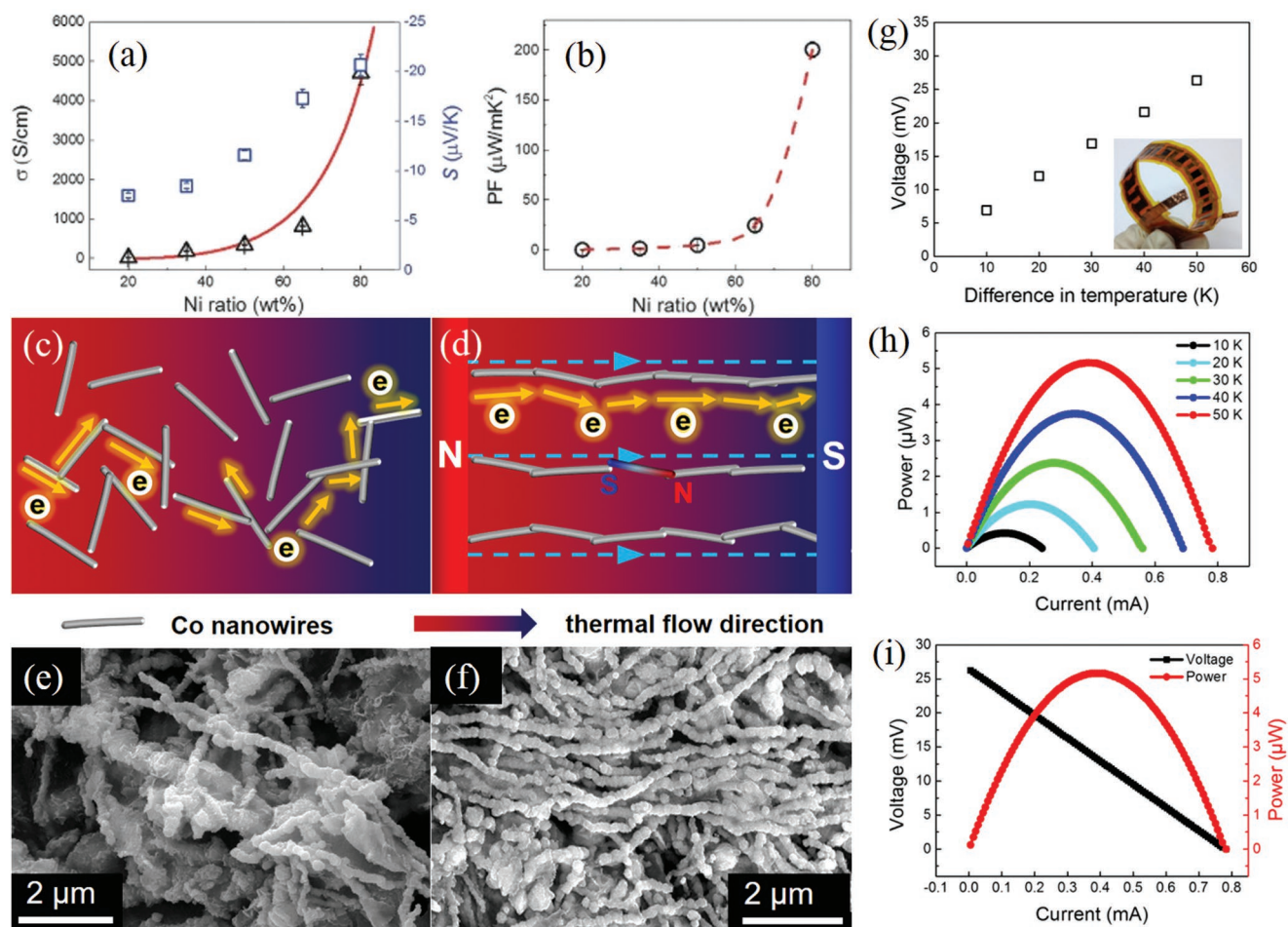


**Figure 11.** a,b) TE performance of Ni NWs/PVDF TENCs as a function of Ni content at room temperature. Reproduced with permission.<sup>[56]</sup> Copyright 2017, Wiley-VCH. Schematic electron transport and SEM images of Co NWs (80 wt%)/PVDF TENCs c,e) without and d,f) with magnetic alignment. g) Output voltage as a function of temperature gradient, with the inset showing the flexibility of the TE module. h) Output power as a function of current under different temperature gradients. i) The voltage–current and power–current curves of the module with a  $\Delta T$  of 50 K. c–i) Reproduced with permission.<sup>[57]</sup> Copyright 2018, Wiley-VCH.

was obtained at 320 K with 44.5 vol% Co NWs under magnetic alignment. Importantly, these TENCs were highly bendable and thus held potential for fabricating flexible TE modules. Thus, we constructed a planar thermoelectric generator (TEG) comprising of ten pairs of n-type Co/PVDF TENCs and p-type PEDOT:PSS thin films with excellent flexibility as shown in the inset of Figure 11g. The open-circuit voltage, the power–current curves, as well as the voltage–current curve under different temperature gradients ( $\Delta T$ ) are shown in Figure 11g–i, pointing out that the maximum output voltage and power reached the values as high as 26 mV and 5.2  $\mu\text{W}$ , respectively.

### 3.3. 2D Layered Superlattice Structure

Inorganic–organic hybrid superlattices provide additional opportunities to inherently modify interfaces in these structures with the goal of promoting carrier transfer and suppressing phonon transport at the same time. Apart from the advanced ALD and molecular-layer deposition (MLD) techniques,<sup>[58]</sup>

organic intercalation offers a facile approach to fabricate inorganic–organic superlattices.

$\text{TiS}_2$  single crystals have been reported to have an ultrahigh PF of 3710  $\mu\text{W m}^{-1} \text{K}^{-2}$  at room temperature.<sup>[59]</sup> However, the  $zT$  value was only 0.16 due to the relatively high  $\kappa$  of 6.8  $\text{W m}^{-1} \text{K}^{-1}$ . The Koumoto group reported the intercalation of organic molecules, hexylammonium (HA) ions,  $\text{H}_2\text{O}$ , and dimethylsulfoxide (DMSO), into the gaps of layered  $\text{TiS}_2$  by electrochemical intercalation and solvent-exchange processes (Figure 12a).<sup>[60]</sup> The as-prepared superlattice films not only became mechanically flexible, but also achieved an in-plane  $\kappa$  of 0.69  $\text{W m}^{-1} \text{K}^{-1}$  owing to quantum confinement between phonons and carriers within the  $\text{TiS}_2$  layers as well as long-range interactions of phonons and the polar molecules. The optimal  $zT$  value of the hybrid superlattice films was as high as 0.2 at 300 K. However, the PF of as-prepared superlattice films decreased to 450  $\mu\text{W m}^{-1} \text{K}^{-2}$  with an  $\sigma$  of 790  $\text{S cm}^{-1}$ . To further improve the PF of the  $\text{TiS}_2$ -based superlattices, a strategy for optimizing carrier concentration was reported by the same group.<sup>[61]</sup> The inorganic  $\text{TiS}_2$  was intercalated by two kinds of organic donors,

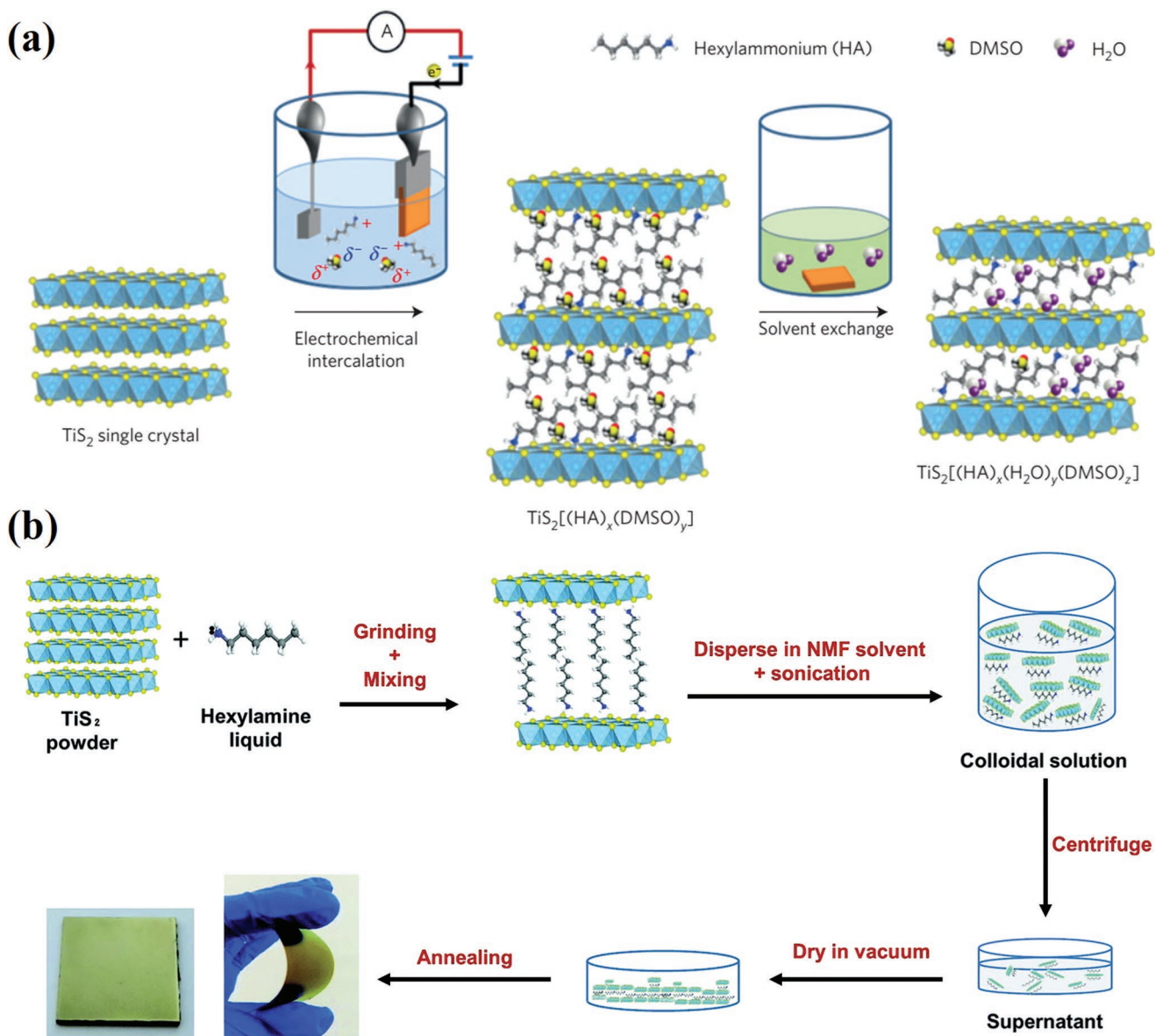


**Figure 12.** a) Synthesis of  $\text{TiS}_2[(\text{HA})_x(\text{H}_2\text{O})_y(\text{DMSO})_z]$  superlattices. Reproduced with permission.<sup>[60]</sup> Copyright 2015, Nature Publishing Group. b) Schematic procedure of flexible  $\text{TiS}_2$ /organic superlattice films. Reproduced with permission.<sup>[62]</sup> Copyright 2017, The Royal Society of Chemistry.

including HA and tetrabutylammonium (TBA). By heating the superlattices at an intermediate temperature between the two boiling points of TBA and HA under vacuum, HA molecules evaporated resulting in a reduction of the carrier density in the  $\text{TiS}_2$  layers. A PF of  $904 \mu\text{W m}^{-1} \text{K}^{-2}$  was obtained when the carrier concentrations were reduced by 2–3 times. Subsequently, this group reported a low-cost liquid-exfoliation and self-reassembly approach, as shown in Figure 12b, to fabricate hybrid  $\text{TiS}_2$ /organic superlattice fabrics. These fabrics consist of alternative layers of  $\text{TiS}_2$  and organic molecules (*N*-methylformamide and hexylamine) and may be suitable for large-scale production.<sup>[62]</sup>

Vanadium pentoxide ( $\text{V}_2\text{O}_5$ ) sol-gels are also suitable matrices for the intercalation of a variety of materials, both organic and inorganic, displaying a lamellar structure. Wu et al.

reported a (polyaniline) $_x\text{V}_2\text{O}_5$  ( $(\text{PANI})_x\text{V}_2\text{O}_5$ ) hybrid material by intercalation of aniline or anilinium and in situ polymerization in  $\text{V}_2\text{O}_5 \cdot n\text{H}_2\text{O}$  xerogels. The  $\sigma$  was in the range of  $10^{-4}$ – $10^{-1} \text{ S cm}^{-1}$  depending on the degree of PANI polymerization and  $S$  varied from  $-200$  to  $-30 \mu\text{V K}^{-1}$ .<sup>[63]</sup> Likewise, Ferhat et al. developed an n-type  $(\text{PEDOT})_x\text{V}_2\text{O}_5$  hybrid superlattice TENCs with good air stability and solution processability.<sup>[64]</sup> They inserted PEDOT into the monolayers of  $\text{V}_2\text{O}_5$  by in situ polymerization of EDOT, which could efficiently enhance the charge carrier concentrations of  $\text{V}_2\text{O}_5$ . The optimal PF of  $2 \mu\text{W m}^{-1} \text{K}^{-2}$  was obtained, which was much higher than that of  $\text{V}_2\text{O}_5$  films ( $2 \times 10^{-3} \mu\text{W m}^{-1} \text{K}^{-2}$ ). Moreover, the hybrid  $(\text{PEDOT})_x\text{V}_2\text{O}_5$  TENCs can be fabricated into mass-scale TE module by inkjet-printing.

## 4. Conclusions and Outlooks

Organic–inorganic thermoelectric nanocomposites have witnessed leap-and-bound advances in research across the globe especially in the past 5 years due to their low-cost and simple solution fabrication at low temperature. Moreover, n-type TENCs have attracted increasing attention given that the performance of n-type TE materials is far behind that of their p-type counterparts. The conclusion can be drawn from this review that there exist different features in CNT- and NC-based n-type TENCs; in other words, the main purpose of hybridizing with organic materials differs between these two types of TENCs. For CNT-based TENCs, the electrical conductivity is relatively high generally due to the intrinsic high conductivity of pristine CNTs and the strong  $\pi$ – $\pi$  interactions at the interfaces of conjugated organic materials and CNTs, which may further increase the conductivity. By taking into account that CNTs present excellent flexibility and can be easily treated in solutions, obtaining both the n-type doping efficiency and the high Seebeck coefficient are two main factors that motivate the fabrication of CNT-based n-type TENCs. Meanwhile, their thermal conductivities are noticeably high, in particular along the in-plane direction. In contrast, for NC-based TENCs, obtaining flexibility and reducing thermal conductivity were the considerations leading to the hybridization with polymers. However, a large amount of NCs is often added to obtain outstanding TE performance, which unfortunately sacrifices the flexibility of TENCs. Strategies sought for optimizing the performance of n-type TENCs so far are reviewed in this article. Still, critical factors hindering the development of n-type TENCs are the air stability, the influence of organic/inorganic interfaces on TE performance, the method of precisely controlling the morphology, as well as largely reducing the content of inorganic components while maintaining the high power factors.

First, the air instability is the biggest issue obstructing the applications of n-type TENCs. To resolve this problem, novel strategies<sup>[23,36]</sup> need to be developed to improve the air- and thermal stability of n-type TENCs. Meanwhile, the encapsulation method of preventing air oxidation for TE devices should be valued, which may be a breakthrough in this long-standing issue troubling researchers. Second, it remains a great challenge to clarify the influence of organic/inorganic interfaces on the performance of n-type TENCs. The interfacial interactions between organic and inorganic components may play a crucial role in the transport of charge carriers and phonons.<sup>[30]</sup> Thus, an in-depth understanding of interfaces would aid in the fabrication of high-performance n-type TENCs at a molecular level. It is worth noting that suitable surface modifiers should be chosen to improve the dispersion of organic and inorganic phases. Third, the current studies on TENCs lack of precise control of morphology. Both the orientation of inorganic NCs along a certain direction<sup>[57]</sup> and the molecular alignment of conducting polymer chains<sup>[65]</sup> would greatly enhance the electrical conductivity of TENCs without sacrificing the Seebeck coefficient, which is due to the obvious increase of carrier mobility, leading to an outstanding power factor. Of course, the thermal conductivity would also rise drastically, which has to be resolved simultaneously. Finally, most of the n-type TENCs with outstanding power factors, no matter CNT- or NC-based ones,

share the common feature that the content of inorganic components is really high. In the case of NC-based n-type TENCs, the high content of inorganic nanocrystals would adversely affect the flexibility of the resulting nanocomposites. Besides, the thermal conductivity would be extremely high in such conditions. As a result, novel methods have to be adopted to reduce the content of inorganic components while maintaining the high PFs.<sup>[66]</sup> Therefore, further research of n-type TENCs should be mainly focused on these four main issues. We hope this review will shed light on the further research thrusts on n-type TENCs.

## Acknowledgements

J.T. and Y.C. contributed equally to this work. This work was sponsored by National Natural Science Foundation of China (NSFC) under Grant No. 51673044 (Z.L.) and International Cooperation Project of Ministry of Science and Technology (MOST) under Grant No. 2017YFE0107800 (Z.L., L.C., and G.B.).

## Conflict of Interest

The authors declare no conflict of interest.

## Keywords

carbon nanotubes, inorganic nanocrystals, layered superlattices, n-type semiconductors, thermoelectric nanocomposites

Received: December 17, 2018

Revised: January 24, 2019

Published online: February 7, 2019

- [1] M. Zebarjadi, K. Esfarjani, M. S. Dresselhaus, Z. F. Ren, G. Chen, *Energy Environ. Sci.* **2012**, *5*, 5147.
- [2] M. Beekman, D. T. Morelli, G. S. Nolas, *Nat. Mater.* **2015**, *14*, 1182.
- [3] Y. Chen, Y. Zhao, Z. Liang, *Energy Environ. Sci.* **2015**, *8*, 401.
- [4] J. He, T. M. Tritt, *Science* **2017**, *357*, 1369.
- [5] C. Xiao, Z. Li, K. Li, P. Huang, Y. Xie, *Acc. Chem. Res.* **2014**, *47*, 1287.
- [6] X. Su, P. Wei, H. Li, W. Liu, Y. Yan, P. Li, C. Su, C. Xie, W. Zhao, P. Zhai, Q. Zhang, X. Tang, C. Uher, *Adv. Mater.* **2017**, *29*, 1602013.
- [7] G. J. Snyder, E. S. Toberer, *Nat. Mater.* **2008**, *7*, 105.
- [8] S. Ortega, M. Ibáñez, Y. Liu, Y. Zhang, M. V. Kovalenko, D. Cadavid, A. Cabot, *Chem. Soc. Rev.* **2017**, *46*, 3510.
- [9] B. Yu, M. Zebarjadi, H. Wang, K. Lukas, H. Wang, D. Wang, C. Opeil, M. Dresselhaus, G. Chen, Z. F. Ren, *Nano Lett.* **2012**, *12*, 2077.
- [10] Y. Pei, J. Lensch-Falk, E. S. Toberer, D. L. Medlin, G. J. Snyder, *Adv. Funct. Mater.* **2011**, *21*, 241.
- [11] Y. Zhou, L.-D. Zhao, *Adv. Mater.* **2017**, *29*, 1702676.
- [12] Q. Zhang, Y. Sun, W. Xu, D. Zhu, *Adv. Mater.* **2014**, *26*, 6829.
- [13] B. Russ, A. Gludell, J. J. Urban, M. L. Chabiny, R. A. Segalman, *Nat. Rev. Mater.* **2016**, *1*, 16050.
- [14] T. O. Poehler, H. E. Katz, *Energy Environ. Sci.* **2012**, *5*, 8110.
- [15] H. Chen, V. V. Ginzburg, J. Yang, Y. Yang, W. Liu, Y. Huang, L. Du, B. Chen, *Prog. Polym. Sci.* **2016**, *59*, 41.
- [16] R. Tian, C. Wan, N. Hayashi, T. Aoai, K. Koumoto, *MRS Bull.* **2018**, *43*, 193.

- [17] J. L. Blackburn, A. J. Ferguson, C. Cho, J. C. Grunlan, *Adv. Mater.* **2018**, *30*, 1704386.
- [18] Q. Yao, Q. Wang, L. Wang, L. Chen, *Energy Environ. Sci.* **2014**, *7*, 3801.
- [19] A. D. Avery, B. H. Zhou, J. Lee, E.-S. Lee, E. M. Miller, R. Ihly, D. Wesenberg, K. S. Mistry, S. L. Guillot, B. L. Zink, Y.-H. Kim, J. L. Blackburn, A. J. Ferguson, *Nat. Energy* **2016**, *1*, 16033.
- [20] W. Zhao, S. Fan, N. Xiao, D. Liu, Y. Y. Tay, C. Yu, D. Sim, H. H. Hng, Q. Zhang, F. Boey, J. Ma, X. Zhao, H. Zhang, Q. Yan, *Energy Environ. Sci.* **2012**, *5*, 5364.
- [21] P. G. Collins, K. Bradley, M. Ishigami, A. Zettl, *Science* **2000**, *287*, 1801.
- [22] W. Zhou, Q. Fan, Q. Zhang, L. Cai, K. Li, X. Gu, F. Yang, N. Zhang, Y. Wang, H. Liu, W. Zhou, S. Xie, *Nat. Commun.* **2017**, *8*, 14886.
- [23] Y. Nonoguchi, M. Nakano, T. Murayama, H. Hagino, S. Hama, K. Miyazaki, R. Matsubara, M. Nakamura, T. Kawai, *Adv. Funct. Mater.* **2016**, *26*, 3021.
- [24] C. Klinke, J. Chen, A. A. Afzali, P. Avouris, *Nano Lett.* **2005**, *5*, 555.
- [25] K. S. Mistry, B. A. Larsen, J. D. Bergeson, T. M. Barnes, G. Teeter, C. Engtrakul, J. L. Blackburn, *ACS Nano* **2011**, *5*, 3714.
- [26] G. Wu, C. Gao, G. Chen, X. Wang, H. Wang, *J. Mater. Chem. A* **2016**, *4*, 14187.
- [27] C. Yu, A. Murali, K. Choia, Y. Ryua, *Energy Environ. Sci.* **2012**, *5*, 9481.
- [28] Y. Ryu, D. Freeman, C. Yu, *Carbon* **2011**, *49*, 4745.
- [29] S. L. Kim, K. Choi, A. Tazebay, C. Yu, *ACS Nano* **2014**, *8*, 2377.
- [30] C. Cho, M. Culebras, K. L. Wallace, Y. Song, K. Holder, J.-H. Hsu, C. Yu, J. C. Grunlan, *Nano Energy* **2016**, *28*, 426.
- [31] Y. Nonoguchi, K. Ohashi, R. Kanazawa, K. Ashiba, K. Hata, T. Nakagawa, C. Adachi, T. Tanase, T. Kawai, *Sci. Rep.* **2013**, *3*, 3344.
- [32] S. M. Kim, J. H. Jang, K. K. Kim, H. K. Park, J. J. Bae, W. J. Yu, I. H. Lee, G. Kim, D. D. Loc, U. J. Kim, E.-H. Lee, H.-J. Shin, J.-Y. Choi, Y. H. Lee, *J. Am. Chem. Soc.* **2009**, *131*, 327.
- [33] C. J. An, Y. H. Kang, H. Song, Y. Jeong, S. Y. Cho, *J. Mater. Chem. A* **2017**, *5*, 15631.
- [34] Y. Nonoguchi, A. Tani, T. Ikeda, C. Goto, N. Tanifuji, R. M. Uda, T. Kawai, *Small* **2017**, *13*, 1603420.
- [35] B. Russ, M. J. Robb, F. G. Brunetti, P. L. Miller, E. E. Perry, S. N. Patel, V. Ho, W. B. Chang, J. J. Urban, M. L. Chabiny, C. J. Hawker, R. A. Segalman, *Adv. Mater.* **2014**, *26*, 3473.
- [36] G. Wu, Z.-G. Zhang, Y. Li, C. Gao, X. Wang, G. Chen, *ACS Nano* **2017**, *11*, 5746.
- [37] C.-Z. Li, C.-C. Chueh, F. Ding, H.-L. Yip, P.-W. Liang, X. Li, A. K.-Y. Jen, *Adv. Mater.* **2013**, *25*, 4425.
- [38] X. Cheng, X. Wang, G. Chen, *J. Mater. Chem. A* **2018**, *6*, 19030.
- [39] B. A. MacLeod, N. J. Stanton, I. E. Gould, D. Wesenberg, R. Ihly, Z. R. Owczarczyk, K. E. Hurst, C. S. Fewox, C. N. Folmar, K. H. Hughes, B. L. Zink, J. L. Blackburn, A. J. Ferguson, *Energy Environ. Sci.* **2017**, *10*, 2168.
- [40] T. Fukumaru, T. Fujigaya, N. Nakashima, *Sci. Rep.* **2015**, *5*, 7951.
- [41] L.-J. Li, A. N. Khlobystov, J. G. Wiltshire, G. A. D. Briggs, R. J. Nicholas, *Nat. Mater.* **2005**, *4*, 481.
- [42] H. Wang, J.-H. Hsu, S.-I. Yi, S. L. Kim, K. Choi, G. Yang, C. Yu, *Adv. Mater.* **2015**, *27*, 6855.
- [43] Y. Li, C.-K. Mai, H. Phan, X. Liu, T.-Q. Nguyen, G. C. Bazan, M. B. Chan-Park, *Adv. Mater.* **2014**, *26*, 4697.
- [44] C.-K. Mai, B. Russ, S. L. Fronk, N. Hu, M. B. Chan-Park, J. J. Urban, R. A. Segalman, M. L. Chabiny, G. C. Bazan, *Energy Environ. Sci.* **2015**, *8*, 2341.
- [45] C. Dun, C. A. Hewitt, H. Huang, J. Xu, D. S. Montgomery, W. Nie, Q. Jiang, D. L. Carroll, *ACS Appl. Mater. Interfaces* **2015**, *7*, 7054.
- [46] B. Zhang, J. Sun, H. E. Katz, F. Fang, R. L. Opila, *ACS Appl. Mater. Interfaces* **2010**, *2*, 3170.
- [47] J. Martin, L. Wang, L. Chen, G. S. Nolas, *Phys. Rev. B* **2009**, *79*, 115311.
- [48] C. Dun, C. A. Hewitt, H. Huang, J. Xu, C. Zhou, W. Huang, Y. Cui, W. Zhou, Q. Jiang, D. L. Carroll, *Nano Energy* **2015**, *18*, 306.
- [49] C. Zhou, C. Dun, B. Ge, K. Wang, Z. Shi, G. Liu, D. L. Carroll, G. Qiao, *Nanoscale* **2018**, *10*, 14830.
- [50] A. A. Rahman, A. A. Umar, M. H. U. Othman, *Phys. E* **2015**, *66*, 293.
- [51] J. We, S. Kim, B. J. Cho, *Energy* **2014**, *73*, 506.
- [52] Y. Wang, K. Cai, X. Yao, *ACS Appl. Mater. Interfaces* **2011**, *3*, 1163.
- [53] Q. Jin, W. Shi, Y. Zhao, J. Qiao, J. Qiu, C. Sun, H. Lei, K. Tai, X. Jiang, *ACS Appl. Mater. Interfaces* **2018**, *10*, 1743.
- [54] Y. Du, J. Chen, X. Liu, C. Lu, J. Xu, B. Paul, P. Eklund, *Coatings* **2018**, *8*, 25.
- [55] M. He, Y. Zhao, B. Wang, Q. Xi, J. Zhou, Z. Liang, *Small* **2015**, *11*, 5889.
- [56] Y. Chen, M. He, B. Liu, G. C. Bazan, J. Zhou, Z. Liang, *Adv. Mater.* **2017**, *29*, 1604752.
- [57] Y. Chen, M. He, J. Tang, G. C. Bazan, Z. Liang, *Adv. Electron. Mater.* **2018**, *4*, 1800200.
- [58] A. J. Karttunen, T. Tynell, M. Karppinen, *Nano Energy* **2016**, *22*, 338.
- [59] H. Imai, Y. Shimakawa, Y. Kubo, *Phys. Rev. B* **2001**, *64*, 241104.
- [60] C. Wan, X. Gu, F. Dang, T. Itoh, Y. Wang, H. Sasaki, M. Kondo, K. Qoga, K. Yabuki, G. J. Snyder, R. Yang, K. Koumoto, *Nat. Mater.* **2015**, *14*, 622.
- [61] C. Wan, R. Tian, M. Kondou, R. Yang, P. Zong, K. Koumoto, *Nat. Commun.* **2017**, *8*, 1024.
- [62] R. Tian, C. Wan, Y. Wang, Q. Wei, T. Ishida, A. Yamamoto, A. Tsuruta, W. Shin, S. Lig, K. Koumoto, *J. Mater. Chem. A* **2017**, *5*, 564.
- [63] C.-G. Wu, D. C. DeGroot, H. O. Marcy, J. L. Schindler, C. R. Kannewurf, Y.-J. Liu, W. Hirpo, M. G. Kanatzidis, *Chem. Mater.* **1996**, *8*, 1992.
- [64] S. Ferhat, C. Domain, J. Vidal, D. Noël, B. Ratiera, B. Lucasa, *Sustainable Energy Fuels* **2018**, *2*, 199.
- [65] S. Qu, Q. Yao, L. Wang, Z. Chen, K. Xu, H. Zeng, W. Shi, T. Zhang, C. Uher, L. Chen, *NPG Asia Mater.* **2016**, *8*, e292.
- [66] W. Shi, S. Qu, H. Chen, Y. Chen, Q. Yao, L. Chen, *Angew. Chem., Int. Ed.* **2018**, *57*, 8037.